The International Journal of Advanced Manufacturing Technology (2024) 133:1609–1620
https://doi.org/10.1007/s00170-024-13795-2

ORIGINAL ARTICLE

AAC theory for ultrasonic vibration-assisted grinding

Zhongwei Hu[1,2] · Yue Chen[1,2] · Zhiyuan Lai[1,2] · Yuqiang Zhang[1,2] · Yiqing Yu[2] · Jianfeng Jin[3] · Qing Peng[4,5] · Xipeng Xu[1,2]

Received: 18 August 2023 / Accepted: 11 May 2024 / Published online: 3 June 2024

Abstract
Ultrasonic vibration-assisted grinding (UVG) has several advantages, such as small grinding force, good surface quality, and high grinding efficiency, outperforming conventional grinding (CG). However, it is sensitive to process parameters, making optimal processing parameters crucial and a major challenge. Therefore, in this study, we introduce a model based on the AAC theory, which uses only three quantities (vibration Angle, contact Area, and influence Coefficient of adjacent abrasive particles) to assess the forces during UVG. These three quantities depend on the movement trajectory, mutual contact relationship between the workpiece and abrasive particles, and spacing between abrasive particles. The effects of these three quantities on the scratch force were examined using molecular dynamics (MD) simulations. The reduction ratios of forces (tangential and normal directions) gradually increased with increasing angle, while the differences in the force reduction ratios for the different contact areas were not significant. As the influence coefficient increased, the reduction ratio of the tangential force increased and then flattened, and the reduction of the normal force increased and then slightly decreased. Spearman's correlation analysis shows that the vibration angle has the most effect on the reduction ratio of the scratch force. And the AAC theory was verified by UVG experiments.

Keywords Ultrasonic vibration-assisted grinding · Molecular dynamics · Scratch force · Process parameters optimization

1 Introduction

The grinding process enables the effective removal of difficult-to-machine materials, which presents a contradiction between machining efficiency and quality. Ultrasonic vibration-assisted grinding (UVG) can effectively solve the problems encountered during the conventional grinding (CG) [1, 2]. UVG can reduce grinding force [3–5], surface roughness [6, 7], and subsurface damage [8, 9], improve material removal rate [10, 11], and reduce tool wear [12], which is applied ultrasonic vibration to a workpiece or tool during CG [13]. Selecting process parameters is important for controlling the UVG machining effect as many parameters are involved in the UVG process, including vibration parameters, machining parameters, abrasive particle parameters, and abrasive particle layout.

A series of single-factor experiments were conducted using theory, simulations, and experiments to study the effects of various parameters on UVG. Concerning the ultrasonic vibration parameters, as the amplitude increases, the oscillation distance of the abrasive particles relative to the balance position increases, increasing the interference between the trajectories of the abrasive particles [14]. These reasons favor the containment of force fluctuation, reducing the grinding force [15–17], while also reducing brittle fracture damage [15, 18]. In addition, amplitude is a crucial factor affecting UVG surface roughness, and increasing amplitude is beneficial for reducing surface roughness [19].

✉ Zhongwei Hu
huzhongwei@hqu.edu.cn

✉ Qing Peng
PengQing@imech.ac.cn

1 Institute of Manufacturing Engineering, Huaqiao University, Xiamen 361021, China

2 Institute of Mechanical Engineering and Automation, Huaqiao University, Xiamen 361021, China

3 Key Laboratory for Anisotropy and Texture of Materials, Northeastern University, Shenyang, China

4 State Key Laboratory of Nonlinear Mechanics, Institute of Mechanics, Chinese Academy of Sciences, Beijing 100190, China

5 School of Engineering Sciences, University of Chinese Academy of Sciences, Beijing 100190, China

With an increase in ultrasonic frequency, the path length of an abrasive particle increases, leading to a reduction in grinding depth. Consequently, the grinding force decreases. Moreover, an increase in frequency also favors a higher speed and lower surface roughness [20].

Regarding the machining parameters, the grinding force decreases with increasing speed [4, 15, 21, 22]. With increasing grinding depth, grinding force increases [6, 8, 15]. While the workpiece feed speed increases, the maximum penetration depth and grinding force increases [6, 15]. As for the abrasive particle parameters, an increase in abrasive particle size leads to a decrease in the amount of active abrasive particles in the same cutting area. Therefore, by increasing the undeformed cutting thickness, the grinding force increases [18]. The arrangement of the abrasive particles significantly influences the surface quality; a suitable special arrangement can improve surface quality and stability [23]. In vibration-assisted scratch (VS) simulations, vibration strengthens the interaction between the abrasive particles. As the spacing of abrasive particles increases, the interaction between them gradually weakens until it disappears [24]. As previously mentioned, each parameter impacts the machining effect. However, some parameters are interdependent, making it difficult to reflect the correlation between parameters in the process of single-factor experiments, considering the coupling effect of the parameters between them is desirable.

Some studies have focused on parameter coupling and optimization. Yu et al. [25] analyzed the influence of abrasive particle diameter, machining time, amplitude, spindle speed, and clearance between the tool and workpiece on surface roughness and material removal rate during ultrasonic vibration-assisted polishing through an orthogonal experiment method. Sharma et al. [26] established a statistical model of residual stress and found that amplitude is the most important parameter affecting residual stress generation. Wang et al. [27] addressed the matching problem between an ultrasonic system and a machine tool system. They provided the abrasive particle motion equation, grinding force prediction model, removal rate model, and a matching model. Sun et al. [28] investigated the relationship between surface roughness and machining parameters, proposed the critical ultrasonic amplitude, and obtained the relationship between the critical ultrasonic amplitude and cutting depth. Lee et al. [29] used an L9 orthogonal array in the Taguchi method to study the influence of tool materials, tool types, abrasive particles, and feed rate on the machining effect. They concluded that all four factors are important in ultrasonic vibration-assisted machining. These studies suggested that it is vital to consider the correlation between the UVG process parameters. The effect of UVG depends largely on the selection of the process parameters, while the effects of different parameter combinations on the results were highly variable. Selecting a reasonable set of parameters to obtain high-quality machining results is challenging. Therefore, to improve machining efficiency and quality, it is crucial to propose a reasonable parameter optimization method for machining difficult-to-machine materials [30, 31]. However, the basic theory for considering the mutual coupling effect between the UVG parameters is lacking.

To fill this gap, we introduce a novel optimization method to summarize the parameters involved in the grinding process. A set of three parameters (referred to as AAC hereafter) of vibration Angle, contact Area, and influence Coefficient of adjacent abrasive particles is proposed to represent all the parameters in the VS. The force reduction ratio is used as the evaluation index to comment the effect of VS. The relationships between machining effect and the parameters were established and verified by MD simulations and UVG experiments.

2 AAC theory

Selecting grinding process parameters is important to obtain an ideal machining effect [24]. However, many parameters are involved in the UVG process, including vibration parameters such as vibration amplitude A and vibration frequency f, machining parameters such as cutting depth a_p and speed v (grinding wheel speed v_s and workpiece feed speed v_w), and abrasive particle size parameters such as abrasive particle radius R and the spacing between abrasive particles d. As shown in Fig. 1, the factors influencing the UVG process can be simplified into three key quantities: (1) the vibration angle reflecting the trajectory of the abrasive particles, (2) the size of the contact area reflecting the contact between the abrasive grain and the workpiece, and (3) the influence coefficient reflecting the interaction of adjacent abrasive particles. We denote the coupling mechanism as the AAC theory to emphasize the three key quantities of vibration Angle, contact Area, and influence Coefficient.

2.1 Vibration angle

The motion equation of the abrasive particle trajectory is shown in Eqs. 1,

$$\begin{cases} x = vt \\ y = A\ sin(2\pi t \times f) \end{cases} \tag{1}$$

The parameters affecting the trajectory of the abrasive particles mainly include amplitude, frequency, and speed. The vibration angle is proposed to count the synergistic effects of the amplitude, frequency, and speed, which directly reflects the trajectory of the abrasive particles. The vibration angle is calculated using the amplitude, frequency, and speed as follows:

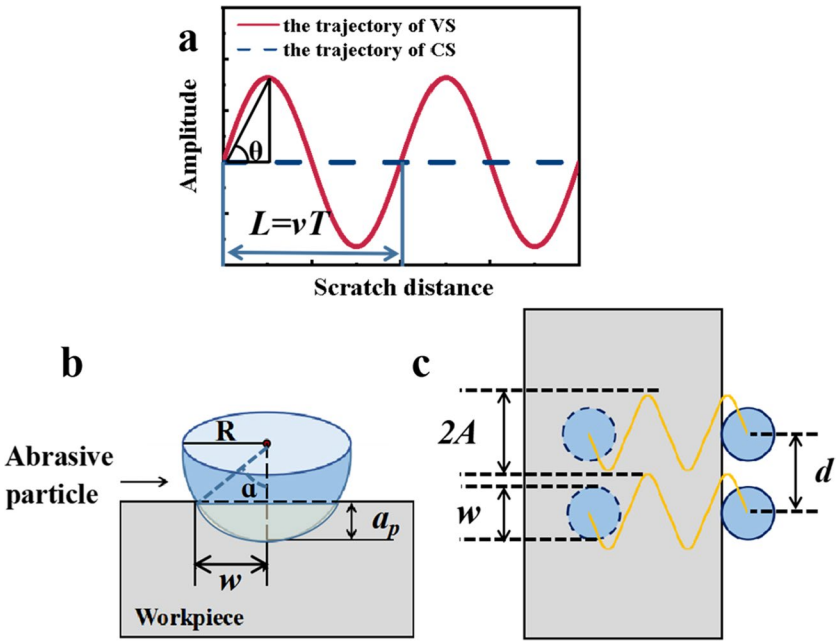

Fig. 1 Schematic diagram of AAC parameter setting: **a** vibration Angle, **b** contact Area, **c** influence Coefficient of adjacent abrasive particles

$$\vartheta = \arctan\frac{A}{\frac{1}{4}L} = \arctan\frac{4A}{(v_s - v_w)T} = \arctan\frac{4Af}{v_s - v_w} \tag{2}$$

where L is the displacement in the x-direction of one cycle of abrasive particle vibration, T is the time of one cycle of abrasive particle vibration, and $f = 1/T$ is the frequency. The change in vibration angle mainly affects the width and density of the trajectory. As the amplitude and frequency increase, the vibration angle also increases. With increasing speed, the vibration angle decreases. The larger the angle, the wider or denser the trajectory of the abrasive particle.

2.2 Contact area

The contact state affects the overlap degree of the abrasive particle trajectory, which further influences the effect of the machining process. Therefore, the combined effects of abrasive particle size and grinding depth are simulated using the contact area. Like Fig. 1b, the contact area is calculated using the grinding depth and abrasive particle radius. The contact area can be calculated:

$$\alpha = \arccos\frac{R - a_p}{R} \tag{3}$$

$$S = \frac{2\alpha}{360^\circ}\pi R^2 - \left(R - a_p\right)R\sin\alpha \tag{4}$$

where α is the center angle corresponding to the contact area.

The contact area increases with an increase in the abrasive particle radius and cutting depth, affecting the degree of overlapping of the abrasive particle trajectory itself during the abrasive particle scratching process.

2.3 Influence coefficient

In Fig. 1c, the mutual interaction between adjacent abrasive particles significantly influences the material removal procedure. The contact width (w) can be obtained based on the cutting depth and radius of the abrasive particles, as shown in Eq. 5.

$$w = 2\sqrt{R^2 - \left(R - a_p\right)^2} \tag{5}$$

It can be seen from experience that the matching degree of the amplitude and width also has a significant impact on the scratching process. An optimal value exists for matching the amplitude and contact width, while the ratio of the amplitude and contact width can be used to evaluate the matching degree of the amplitude and abrasive particle size. The greater the spacing between the abrasive particles, the weaker the interaction between them [24] as shown in Eq. (6), for defining the influence coefficient of the adjacent abrasive particles as

$$c = \frac{2A}{dw} \tag{6}$$

The influence coefficient of adjacent abrasive particles is directly proportional to the amplitude and inversely proportional to the spacing and contact width of the abrasive particles. The change in the influence coefficient of adjacent abrasive particles mainly shows a matching relationship between amplitude, cutting depth, abrasive particle radius,

and abrasive particle spacing and comprehensively considers the relationship between the vibration parameters, machining parameters, abrasive particle size, and abrasive particles layout.

3 Simulation and experiments settings

3.1 Molecular dynamics simulations

Single abrasive particle scratching experiments focus on the interaction mechanism between the abrasive particles and the workpiece [32, 33], while double abrasive particle scratching experiments focus on the coupling interaction between abrasive particles [34, 35]. Studying the scratching process of abrasive particles using molecular dynamics (MD) simulation is a mainstream research method [36]. MD simulation models of single and double abrasive particle scratching were established to study the AAC theory. The relationship between AAC and scratch force was established to guide the process optimization during the UVG experiment and maximize the machining effect.

A typical hard and brittle material, 4 H-SiC, was chosen as the model for this study, while an MD model of 4 H-SiC was built. The workpiece size of the single abrasive particle simulation model was $30 \times 30 \times 15$ nm^3. The abrasive particle radius was 4.0 nm and the cylinder height was 6.0 nm. The workpiece size of the double abrasive particle simulation model was $20 \times 38 \times 7.8$ nm^3. The radius of the hemisphere of the abrasive particles was 2.0 nm. The height of the cylinder was 2.2 nm (Fig. 2). The material of the abrasive particles are all carbon atoms with a perfect diamond crystal lattice, which were fixed as rigid bodies during the scratching process. The Si face of 4 H-SiC was the surface scratched by an abrasive particle. Each parameter was randomly matched within a certain range to set different parameters. For the calculations, we set a series of different angles, two types of contact areas, and different adjacent abrasive coefficients. The simulation parameters are listed in Tables S1 and S2 in the Supplementary Information.

A large-scale atom/molecule massively parallel simulator (LAMMPS) was used to simulate in this paper [37]. The visualization software used the OVITO visualization software [38]. The Tersoff potential function [39] was used in the simulations, and it can describe the interaction between atoms in covalent systems accurately. In the scratching stage, in order to make the scratching under stable external conditions, NVT ensemble was applied to the atoms in the constant temperature layer to keep the temperature of the atoms in the constant temperature layer stable. At the same time, the change of heat should be considered in the process of processing, so the NVE ensemble was applied to the Newton layer atoms. And the time step was set as 0.001 ps.

The scratch force results obtained through the MD simulation are shown in Fig. 3a. The scratch force was averaged in the stable stage (9–15 nm), and the force-reduction ratio (ρ) is defined as follows:

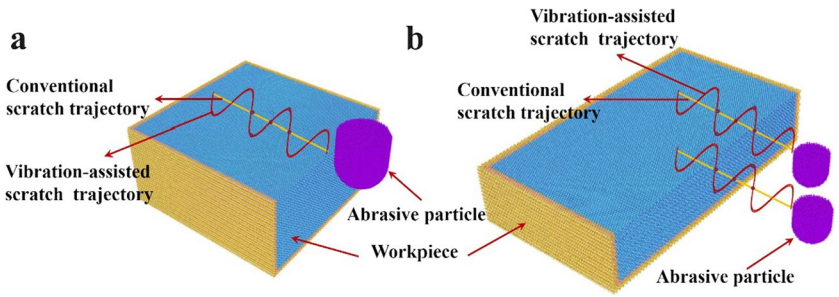

Fig. 2 MD simulation model: (**a**) single abrasive particle and (**b**) double abrasive particle

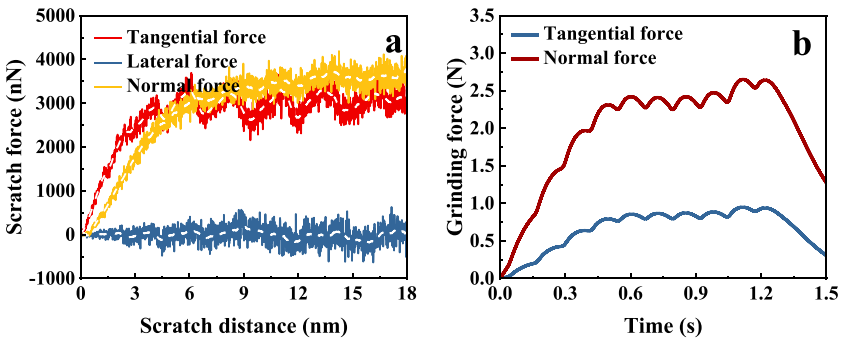

Fig. 3 **a** MD simulation scratch force and **b** results of UVG force

$$\rho = \frac{F_{cs} - F_{VS}}{F_{CS}} \times 100\% \quad (7)$$

where F_{cs} and F_{VS} are the forces in conventional scratch (CS) and VS, respectively. And ρ_t and ρ_n denote the reduction ratio of the tangential force and the reduction ratio of the normal force, respectively.

3.2 Ultrasonic vibration-assisted grinding experiments

To verify the relationship between the three key quantities (AAC) established in the MD and the machining effect, UVG experiments were used to verify and guide the UVG experiment to study the vibration angle on the machining effect. The experiments were conducted using a high-precision surface grinder (Planomat HP 408). The sample was Si-faced SiC with dimensions of $10\times10\times6$ mm^3 and a machined surface of 10×6 mm^2. The details of this device are presented in Fig. 4.

To control the cutting depth of single abrasive particle within the same range, refer to the formula for the maximum cutting thickness: $a_{gmax} = 2\lambda\frac{v_w}{v_s}\sqrt{\frac{a_p}{d_s}}$ [40]. The speed ratio was the same for the different cut depths. The ρ_t and ρ_n were compared with that at the same depth of cut range. The setting of experimental parameters is to set the corresponding vibration angle within the range of experimental device parameters. The vibration frequency was set to 28 kHz to achieve a more even distribution of the vibration angle. The grinding wheel speed was 0.1–2.5 m/s and the workpiece feed rate was 60–1500 mm/min. The speed ratio was 100, amplitude was 0–6 μm, and cut depth was 4–12 μm. The grinding parameters are listed in Table S3 in the Supplementary Information. Forces were measured using a dynamometer (Kistler 9257 B), while surface roughness values were measured using a 3D optical surface profiler (Zygo NewView 7300); the surface topography was imaged by scanning electron microscopy (Phenom).

The results of the grinding force measured using a force-measuring instrument are shown in Fig. 3b. The average grinding force was calculated at the stable stage. The ρ_t and $\rho_n$was then calculated using Eq. 7.

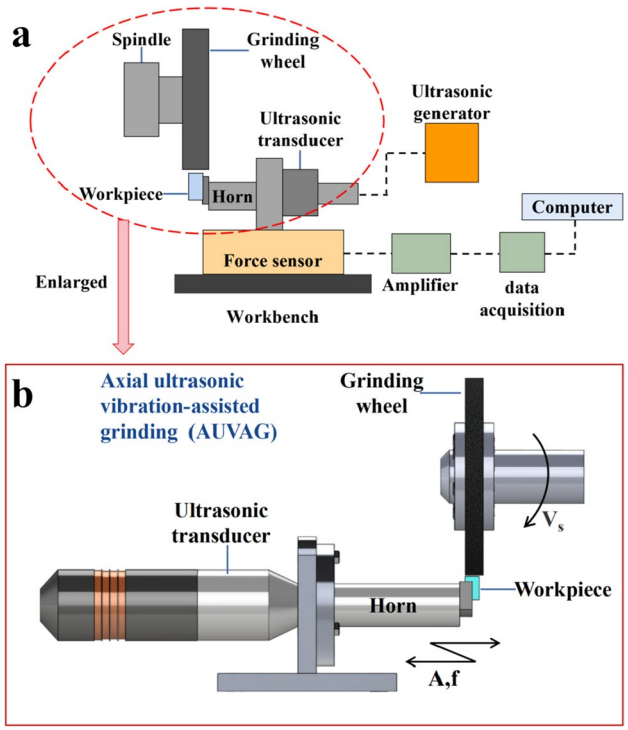

Fig. 4 (a) The experimental device schematic diagram and (b) ultrasonic vibration applied in the axial directions to assist SiC grinding

4 Results

During processing, the magnitude of the scratch force directly affects surface quality, subsurface damage, tool wear, and processing temperature [16, 41]. Compared with CS, numerous studies have shown that the tangential and normal forces in VS are significantly reduced [42]. The effect of VS can be determined by comparing the reduction ratios of the forces (ρ_t and ρ_n); a larger reduction ratio of the scratch force indicates a more significant effect in the VS. Therefore, the scratch force reduction ratio was used to measure the effect of vibration-assisted scratching.

4.1 Effect of vibration angle

A series of single abrasive particle scratching MD simulations were performed to investigate the effect of vibration angle on the scratch force reduction ratio. According to Fig. 5, as the angle increases, the ρ_t and ρ_n gradually increase, and the effect of vibration application gradually becomes significant. The ρ_t is greater than ρ_n. The ρ_t gradually increases from 3.65 to 86.35%, while that of the ρ_n gradually increases from 4.33 to 84.51%.

As the angle increases, the increment ratio of lateral forces first increases and then decreases because, as the angle increases, the trajectory of the abrasive particle movement becomes denser, and the initial scratch angle of the abrasive particles is also closer to the Y direction; the impact of the abrasive particles on the workpiece atoms in the Y direction is stronger, so the lateral force will increase and the increment ratio will increase. When the vibration angle increases to a certain range, the repeated removal ratio of abrasive particles also increases, suggesting that the increase in the ratio of the lateral force gradually decreases. The ρ_t and ρ_n promotes the improvement of the machining effect, while

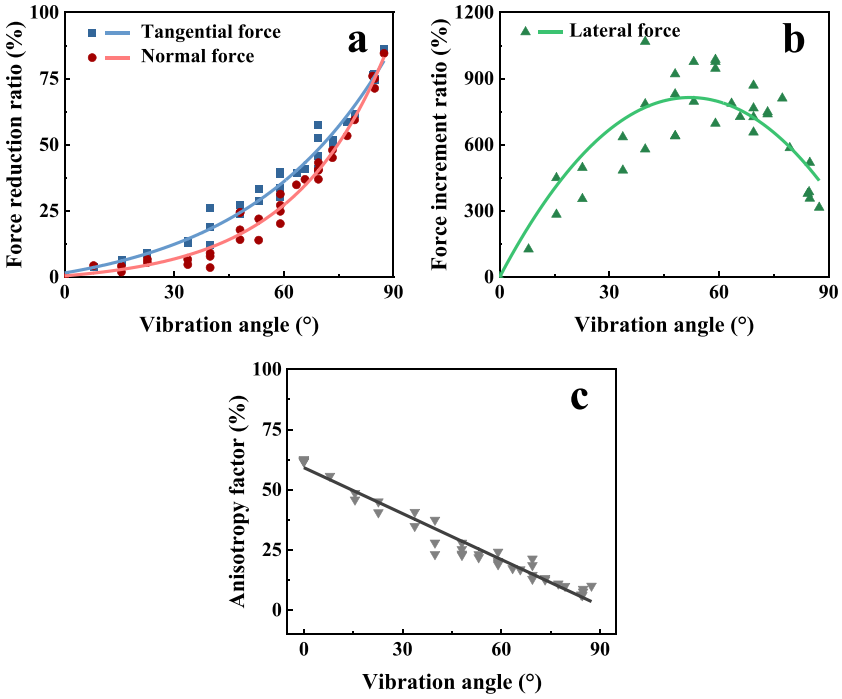

Fig. 5 Relationship between vibration angle and **a** tangential force and normal force reduction ratio(ρ_t and ρ_n), **b** lateral force increment ratio, and **c** anisotropy factor

the increase of the lateral force is beneficial for material removal, increasing the material removal area and improving the machining efficiency. Figure 5 shows that for the same angle, the ρ_t and ρ_n are the same with small fluctuations.

The anisotropy coefficient is used to assess the balance of the distribution of tangential, normal, and lateral forces in the three directions; it is more uniform in three directions and easier to obtain a good machining effect [36]. According to the calculation, the anisotropy factor gradually decreases with increasing angle, as shown in Fig. 5c.

4.2 Effect of contact area

Single abrasive particle scratching MD simulations were performed to study the effect of contact area on the reduction ratio of scratching force. Limited by the model size, the contact area could only be adjusted within a small range. Therefore, within this adjustable range, two contact areas with large gaps were selected for comparison.

Changing the cutting depth and abrasive particle radius alters the contact area, and the degree of overlapping of the abrasive particle itself during the scratching process and thus affects the machining effect are modified. In Fig. 6, with the change in the contact area, the variation of the ρ_t is not significant when the contact area is large, and when the contact area increases, ρ_n increases slightly.

4.3 Effect of influence coefficient

The grinding process is the overall effect of numerous abrasive particles. A series of double abrasive particle scratching simulations were conducted to model the coupling effect.

As shown in Eq. 5, the coefficient of influence of the adjacent abrasive particles is proportional to the amplitude and

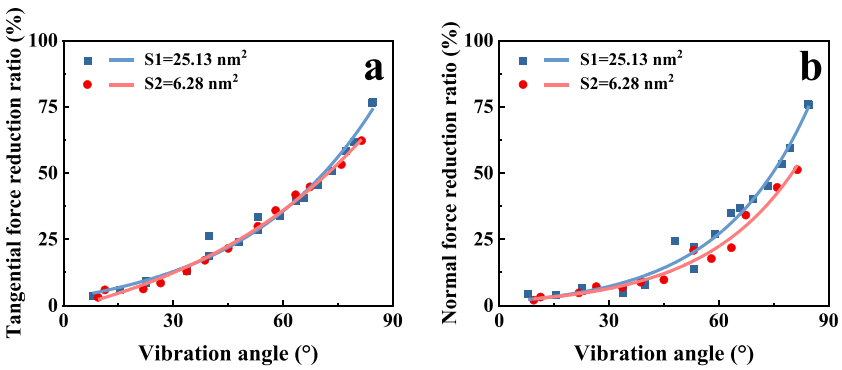

Fig. 6 Effect of contact area on the **a** ρ_t and **b** ρ_n

the spacing between the abrasive particles and the contact width was inversely proportional. In Fig. 7, it can be seen that as the influence coefficient of adjacent abrasive particles increases, the ρ_t gradually increases. After increasing to a certain extent, the ρ_t is gentle or decreases slightly. The ρ_n gradually increases, and after increasing to a certain extent, it decreases. This is because the larger the influence coefficient, the greater the ratio of amplitude to contact width ($\frac{A}{w}$). At this time, the vibration effect of abrasive particles is more significant. And the spacing between abrasive particles (d) is smaller. At this time, the spacing between abrasive particles is closer, making it easier for them to affect each other, so the ρ_t and ρ_n are more significant. However, there is an optimal match between the $\frac{A}{w}$ and the d; otherwise, the influence coefficient will continue to increase and the reduction ratio will not continue to increase. Compared to the condition of large vibration angles, the degree of force reduction is more significant. Because when the angle is large, the impact of vibration angle on the entire scratch process is more significant, so the degree of reduction of ρ_t and ρ_n is smaller than in the case of small vibration angles. In Fig. 7, with the increase in the influence coefficient of adjacent abrasive particles, a larger gap between the amplitude of the abrasive particles and the contact width results in a smaller separation between abrasive particles. The results indicate that when the influence coefficient increases gradually, the ρ_t increases gradually and tends to be flat. The ρ_n increases gradually and then slightly decreases because, at the initial stage, the influence coefficient increases and the degree of influence between the abrasive particles also increases. Consequently, the ρ_t and ρ_n gradually increase. However, when the influence coefficient achieves a certain value, the increase in the influence coefficient may be caused by the small separation between the abrasive particles. The debris on both sides hindered the advancement of the abrasive particles. Therefore, the scratch force increased, and the ρ_t and ρ_n were slightly reduced.

4.4 Correlation analysis

The relationships between the vibration angle, contact area, influence coefficient of adjacent abrasive particles, and the reduction ratio of the scratch force were obtained through vibration-assisted single and double abrasive particle scratching simulations. Spearman's correlation analysis [43] was performed.

As seen in Fig. 8, the interaction between abrasive particles is considered, with the vibration angle exerting the most influence on the change in scratch force. The contact area had little effect on the change in scratch force in the

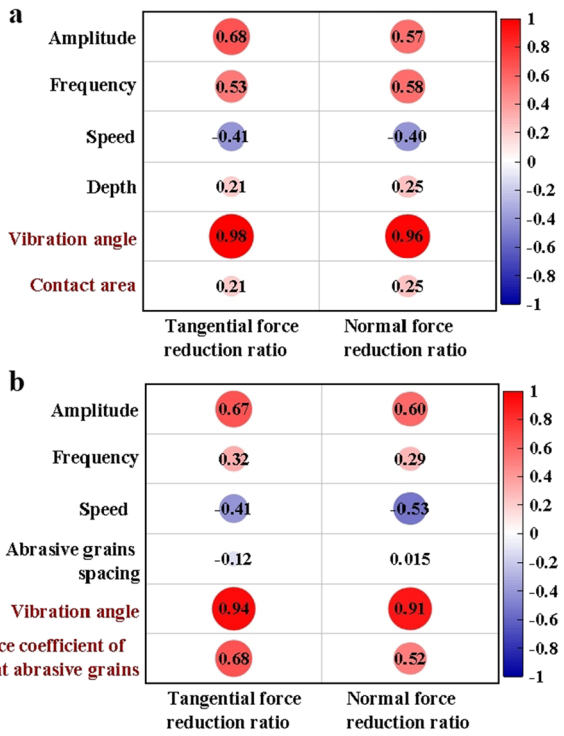

Fig. 8 Correlation analysis of vibration angle, contact area, influence coefficient of adjacent abrasive particles, and scratch force reduction ratio, **a** without considering the interaction and **b** considering the interaction between abrasive particles

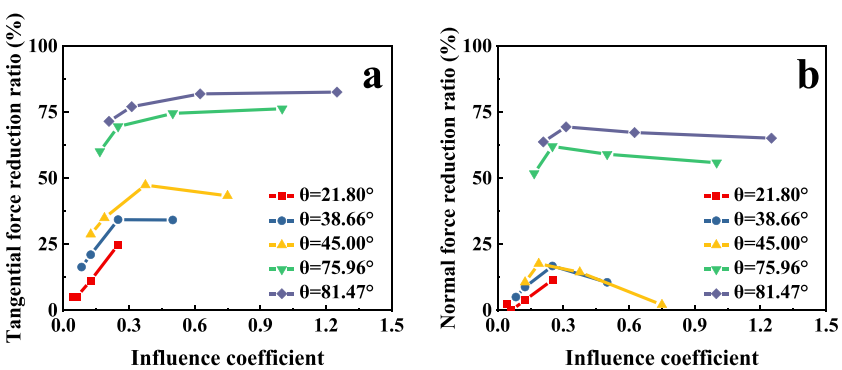

Fig. 7 Effect of influence coefficient between adjacent abrasive particles on the reduction ratio of tangential force and normal force

examined range. Compared to the spacing between the abrasive particles, the effect of the influence coefficient on the change of the scratch force is more prominent.

4.5 Experimental results

Through MD simulations, the relationship between the vibration angle, contact area, influence coefficient, and the scratch force reduction ratio (ρ_t and ρ_n) can be obtained. From the correlation analysis, we can observe that the vibration angle has the most impact on the scratch force. Therefore, in the UVG experiments, we mainly studied the effect of the vibration angle on the grinding process. Simultaneously, the contact area can be changed by changing the grinding depth.

As seen in Fig. 9, throughout the experiment, with increasing vibration angle, the ρ_t and ρ_n increase gradually. Additionally, a linear increasing trend can be observed. The ρ_t gradually increases from 3.01 to 89.99%, and the ρ_n gradually increases from 2.32 to 61.64%. Compared with the single abrasive particle scratching simulation, the shape of the curve changed from a concave curve to a straight line because the grinding process is a comprehensive process of numerous abrasive particles. UVG enhances the interaction between abrasive particles, and the interaction increases the ρ_t and ρ_n and then changes the shape of the curve.

The roughness values of several points were measured randomly on each workpiece, and the surface roughness reduction ratio was calculated. From Fig. 10, it can be seen that as the angle increases, the surface roughness reduction ratio increases gradually. And the surface morphology of the two groups at different angles was compared; the first group is 0 ° (v_s=2 m/s, v_w=1200 mm/min, a_p=8 μm) and 18.75 ° (v_s=2 m/s, v_w=1200 mm/min, a_p =8 μm, f =28 kHz, A=6 μm). The second group is 0 ° (v_s=0.1 m/s, v_w=60 mm/min, a_p=8 μm) and 77.54 ° (v_s=0.1 m/s, v_w =60 mm/min, a_p=8 μm, f=28 kHz, A=4 μm). By comparing the two groups of images, it can be clearly seen that after applying vibration, the surface quality has significantly improved, the number of large cracks was reduced, and the depths of the pit were also reduced. Meanwhile, by reducing the depth of the pits and the number and length of cracks, it can be observed that the larger the increase in vibration angle, the more significant the improvement in surface quality.

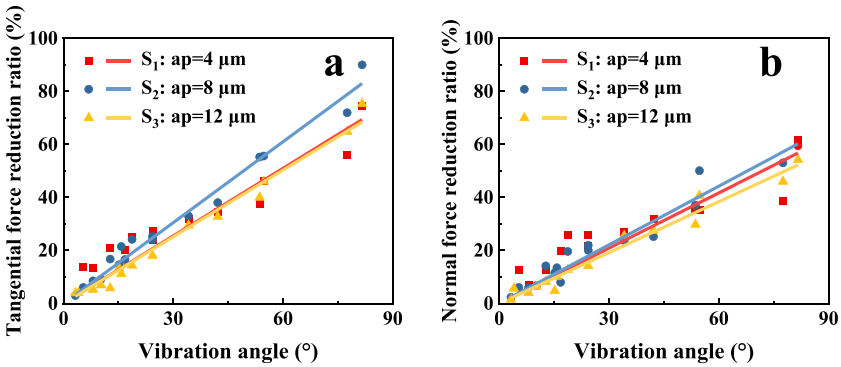

Fig. 9 Relation between grinding force reduction ratio and vibration angle for different contact areas, where $S_1 < S_2 < S_3$

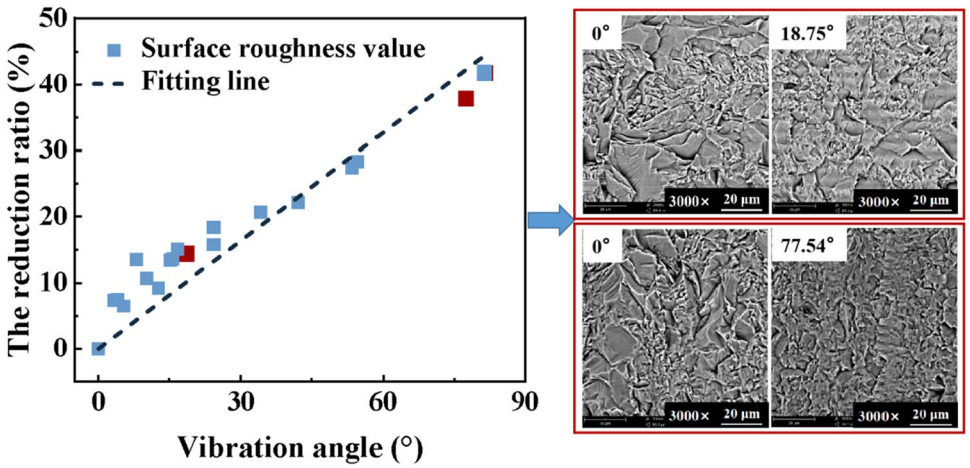

Fig. 10 Relation between vibration angle and surface roughness

5 Discussion

In the VS process, the most intuitive and significant difference compared with CS is the change in trajectory. The application of vibration increases the area of the trajectory of a single abrasive particle. In addition, the trajectory of the abrasive particles overlaps, as shown in Fig. 11. We propose two indicators to quantify this change, i.e., area ratio and interference ratio, enabling us to analyze the mechanism of the ρ_t and ρ_n during the scratching process. The calculation is based on the actual scratching area and theoretical scratching area. The calculation includes both the area ratio (μ) and interference ratio (δ), which are defined as follows:

$$\mu = \frac{S_{\mathrm{VS}} - S_{\mathrm{CS}}}{S_{\mathrm{VS}}} \times 100\% = \frac{S_{\mathrm{VS}} - wl_{\mathrm{CS}}}{S_{\mathrm{VS}}} \times 100\% \tag{8}$$

$$\delta = \frac{wl_{\mathrm{VS}} - S_{\mathrm{VS}}}{wl_{\mathrm{VS}}} \times 100\% \tag{9}$$

where S_{VS} denotes the actual machining area in the VS. S_{CS} is the processing area in the CS; w is the contact width; and l_{CS} and l_{VS} are the trajectory lengths of CS and VS, respectively.

The area ratio μ is the ratio between the actual processing areas of the VS and CS, accounting for the degree of increase in the processing area compared to the CS under the same cutting depth and speed. Therefore, the area ratio μ reflects the degree of increase in processing efficiency. A larger area ratio indicates a larger machining area, which helps improve the machining efficiency. The interference ratio is the ratio of the actual machining area to the theoretical machining area. For CS, the interference ratio is zero because the tracks do not overlap. The interference ratio reflects the overlap of the tracks themselves during vibration-assisted scratching. A large degree of trajectory overlap represents an increase in the repeated machining

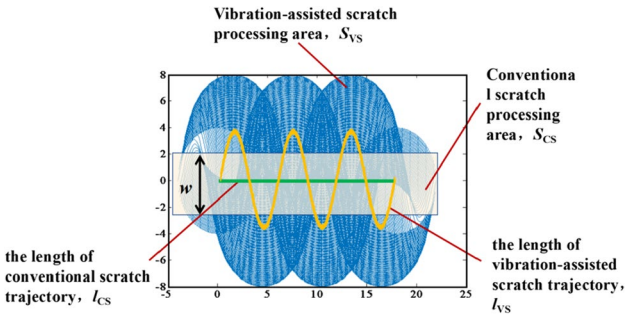

Fig. 11 Schematic diagram of interference ratio and area ratio calculation

area of the abrasive particles, which favors the ρ_t and ρ_n and the improvement of the surface quality.

During the scratching of the two abrasive particles, the overlapping part of the two abrasive particle tracks was calculated based on the overlapping degree of the abrasive particle tracks. The overlapping part represents the part repeatedly removed by two abrasive particles; this overlap ratio is the interference ratio [19].

Considering the vibration angle has the strongest correlation among the three parameters, the relationship between the area ratio interference ratio, vibration angle, and ρ_t and ρ_n in the MD simulation parameters was calculated. The area ratio and interference ratio can be used to scale the ρ_t and ρ_n and to assess the effect of UVG.

In Fig. 12, the vibration angle gradually increases, and the ρ_t and ρ_n gradually increase with an increase in the area ratio. When the vibration angle is less than 40°, the increase in the angle has no significant effect on the interference ratio. When the angle is greater than 40 °, an increase in the angle significantly increases the interference ratio. As a result, the speed of the overlapping degree of the trajectory increases. Consequently, with an increase in the interference ratio, the ρ_t and ρ_n gradually increase. An increase in the angle is beneficial for increasing the area and interference ratios. Therefore, reducing the scratch force and increasing processing efficiency is advantageous.

During the scratching of two abrasive particles, the overlap ratio increases with an increase in the influence coefficient of adjacent abrasive particles (Fig. 12c). In the initial stage, the increasing speed is high, and then gradually tends to plateau, consistent with the change law of the tangential force reduction ratio. Therefore, a larger area where two abrasive particles are repeatedly removed is more conducive to reducing tangential and normal forces. However, after the overlap ratio became constant because of the increase of the adjacent abrasive particle coefficient, the abrasive particles were also more susceptible to the impact of debris accumulation. Consequently, the ρ_t and ρ_n increased slightly.

Using the experimental parameters, the relationships between the area ratio, interference ratio, and vibration angle were examined (Fig. 13). With an increase in the angle, the area ratio and interference ratio gradually increase. When the contact area is large, the area and interference ratios are relatively small; however, the difference between these ratios within the existing cutting depth range is small. Therefore, owing to errors and other reasons in the experiment, it is impossible to clearly show the size relationship of the force-reduction ratio under different cutting depths.

The experimental results validated the MD simulation results. The simulation results show that an increase in the vibration angle favors an increase in the area and interference ratios, as well as the ρ_t and ρ_n, agreeing well with the experiment. The simulation and experimental results showed

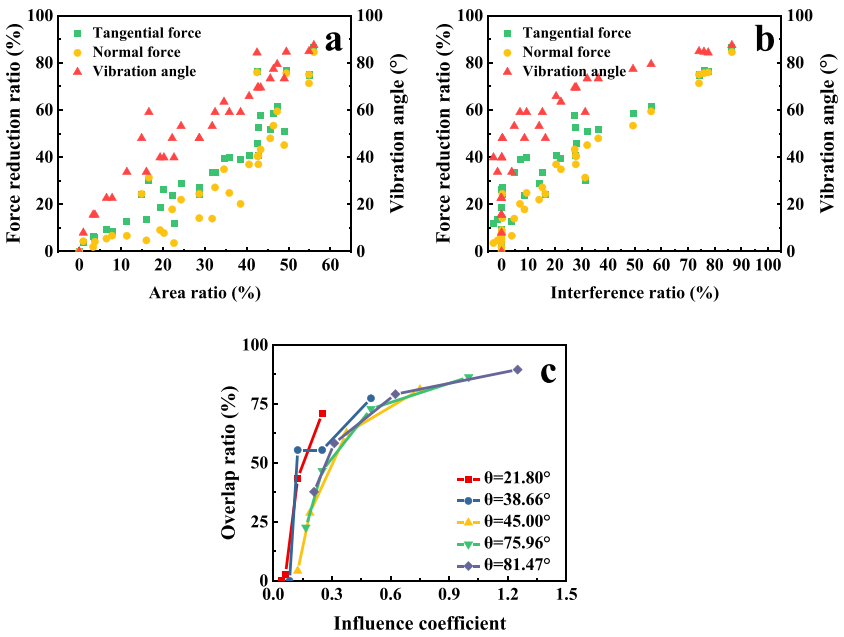

Fig. 12 Relationship between **a** area ratio, **b** interference ratio, and vibration angle and reduction ratio of scratch force. Relationship between **c** influence coefficient and overlap ratio

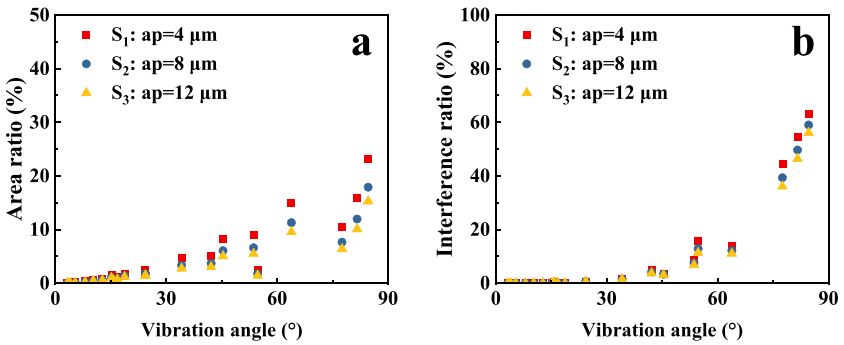

Fig. 13 Relationship between **a** area ratio and **b** interference ratio and vibration angle under experimental parameters, where $S_1 < S_2 < S_3$

the same trend. Therefore, the MD simulations predicted the machining effect of the UVG experiments well.

6 Conclusions

We have introduced the AAC theory $Q = f(\theta, S, c)$, which uses three key quantities (vibration angle θ, contact area S, and influence coefficient c) to assess the performance of the UVG process Q. The influence of these three quantities on the scratch force was investigated by MD simulations. The AAC theory was verified by UVG experiments.

In our AAC theory, the vibration angle θ is used to measure the change in the abrasive particle trajectory. The contact area S describes contact degree between the abrasive particles and the workpiece. The influence coefficient c describes the matching relationship between the spacing of the abrasive particles, the amplitude, and the contact area. We assumed that these three quantities are sufficient for describing and accessing the grinding process.

Through MD simulations, with an increase in the vibration angle, the ρ_t and ρ_n gradually increased and the anisotropy factor of the force gradually decreased. Simultaneously, no obvious differences were observed in the ρ_t and ρ_n in the existing range of contact area changes. An optimal matching relationship between spacing of abrasive particles, amplitude, and contact area was observed. With an increase in the influence coefficient, the ρ_t and ρ_n reached a maximum.

Spearman's correlation analysis showed that the vibration angle had the greatest influence on the ρ_t and ρ_n and the grinding process performance. Simultaneously, through verification of the UVG experiments, it can be found that the increase in vibration angle has a significant impact on the grinding force and surface quality during the machining process. And the change of the ρ_t and ρ_n is consistent with the results obtained from the MD simulation. Subsequent research will continue to focus on vibration angle and abrasive particle arrangement, which can better optimize the vibration-assisted grinding process.

We conclude that the vibration angle, contact area, and influence coefficient of adjacent abrasive particles can be used as an essential basis for optimizing UVG machining parameters. Our AAC theory may provide a feasible and reliable approach for optimizing UVG processes. The validated AAC theory can also guide parameter selection and optimization of UVG processing of hard and brittle materials.

Supplementary Information The online version contains supplementary material available at https://doi.org/10.1007/s00170-024-13795-2.

Funding This work was supported by the National Natural Science Foundation of China (Grant No. 52175404) and The Foreign Cooperation Projects of Fujian Province (Grant No. 2021I0017). Q. P. would also like to acknowledge the support provided by National Natural Science Foundation of China (Grant No. 12272378), and LiYing Program of the Institute of Mechanics, Chinese Academy of Sciences (Grant No. E1Z1011001).

Data availability The datasets generated during and/or analyzed during the current study are available from the corresponding author on reasonable request.

Declarations

Conflict of interest The authors declare no competing interests.

References

1. Lu K, Tian YL, Liu CF, Guo ZY, W FJ, Zhang DW, Shirinzadeh B (2021) Experimental investigation of the effects of vibration parameters on ultrasonic vibration-assisted tip-based nanofabrication. Int J Mech Sci 198:106387. https://doi.org/10.1016/j.ijmecsci.2021.106387
2. Zhou WH, Tang JY, Chen HF, Shao W (2019) A comprehensive investigation of surface generation and material removal characteristics in ultrasonic vibration assisted grinding. Int J Mech Sci 156:14–30. https://doi.org/10.1016/j.ijmecsci.2019.03.026
3. Chen Y, Hu ZW, Yu YQ, Lai ZY, Zhu JG, Xu XP, Peng Q (2022) Processing and machining mechanism of ultrasonic vibration-assisted grinding on sapphire. Mat Sci Semicon Proc 142:106470. https://doi.org/106470
4. Liang ZQ, Wang XB, Wu YB, Xie LJ, Jiao L, Zhao WX (2013) Experimental study on brittle–ductile transition in elliptical ultrasonic assisted grinding (EUAG) of monocrystal sapphire using single diamond abrasive grain. Int J Mach Tool Manu 71:41–51. https://doi.org/10.1016/j.ijmachtools.2013.04.004
5. Yang ZC, Zhu LD, Lin B, Zhang GX, Ni CB, Sui TY (2019) The grinding force modeling and experimental study of ZrO2 ceramic materials in ultrasonic vibration assisted grinding. Ceram Int 45(7):8873–8889. https://doi.org/10.1016/j.ceramint.2019.01.216
6. Chen JB, Fang QH, Li P (2015) Effect of grinding wheel spindle vibration on surface roughness and subsurface damage in brittle material grinding. Int J Mach Tool Manu 91:12–23. https://doi.org/10.1016/j.ijmachtools.2015.01.003
7. Guo B, Zhao Q (2017) Ultrasonic vibration assisted grinding of hard and brittle linear micro-structured surfaces. Precis Eng 48:98–106. https://doi.org/10.1016/j.precisioneng.2016.11.009
8. Wang Y, Liang ZQ, Zhao WX, Wang XB, Wang H (2020) Effect of ultrasonic elliptical vibration assistance on the surface layer defect of M-plane sapphire in microcutting. Mater Des 192:108755. https://doi.org/10.1016/j.matdes.2020.108755
9. Qu W, Wang K, Miller MH, Huang Y, Chandra A (2000) Using vibration-assisted grinding to reduce subsurface damage. Precis Eng 24(4):329–337. https://doi.org/10.1016/S0141-6359(00)00043-X
10. Sun GY, Shi F, Zhao QL, Ma Z, Yang DL (2020) Material removal behaviour in axial ultrasonic assisted scratching of Zerodur and ULE with a Vickers indenter. Ceram Int 46(10):14613–14624. https://doi.org/10.1016/j.ceramint.2020.02.262
11. Qu S, Wang ZX, Zhang C, Ma ZL, Zhang TQ, Chen H, Wang Z, Yu TB, Zhao J (2021) Material removal profile prediction and experimental validation for obliquely axial ultrasonic vibration-assisted polishing of K9 optical glass. Ceram Int 47(23):33106–33119. https://doi.org/10.1016/j.ceramint.2021.08.212
12. Liang ZQ, Wang XB, Wu YB, Xie LJ, Liu ZB, Zhao WX (2012) An investigation on wear mechanism of resin-bonded diamond wheel in elliptical Ultrasonic assisted grinding (EUAG) of monocrystal sapphire. J Mater Process Tech 212(4):88–876. https://doi.org/10.1016/j.jmatprotec.2011.11.009
13. Singh AK, Kumar A, Sharma V, Kala P (2020) Sustainable techniques in grinding: state of the art review. J Clean Prod 269:121876. https://doi.org/10.1016/j.jclepro.2020.121876
14. Zhang MH, Pang ZX, Jia YX, Shan CW (2022) Understanding the machining characteristic of plain weave ceramic matrix composite in ultrasonic-assisted grinding. Ceram Int 48(4):5557–5573. https://doi.org/10.1016/j.ceramint.2021.11.100
15. Dai CW, Yin Z, Wang P, Miao Q, Chen JJ (2021) Analysis on ground surface in ultrasonic face grinding of silicon carbide (SiC) ceramic with minor vibration amplitude. Ceram Int 47(15):21959–21968. https://doi.org/10.1016/j.ceramint.2021.04.214
16. Lei XF, Xiang DH, Peng PC, Liu GF, Li B, Gao GF (2022) Establishment of dynamic grinding force model for ultrasonic-assisted single abrasive high-speed grinding. J Mater Process Tech 300:117420. https://doi.org/10.1016/j.jmatprotec.2021.117420
17. Meng Q et al (2023) Dynamic force modeling and mechanics analysis of precision grinding with microstructured wheels. J Mater Process Tech 314:117900. https://doi.org/10.1016/j.jmatprotec.2023.117900
18. Huang C, Zhou M, Zhang H (2022) Investigations on the micro-interactions of grit-workpiece and forces prediction in ultrasonic vibration side grinding of optical glass. J Mater Process Tech 300:117415. https://doi.org/10.1016/j.jmatprotec.2021.117415
19. Chen YR, Su HH, Qian N, He JY, Gu JQ, Xu JH, Ding K (2021) Ultrasonic vibration-assisted grinding of silicon carbide ceramics based on actual amplitude measurement: grinding force and surface quality. Ceram Int 47(11):15433–15441. https://doi.org/10.1016/j.ceramint.2021.02.109
20. Wang H, Hu YB, Cong WL, Burks AR (2019) Rotary ultrasonic machining of carbon fiber–reinforced plastic composites: effects of ultrasonic frequency. Int J Adv Manuf Tech 104(9–12):3759–3772. https://doi.org/10.1007/s00170-019-04084-4
21. Wang Y, Lin B, Cao XY, Wang SL (2014) An experimental investigation of system matching in ultrasonic vibration assisted grinding for titanium. J Mater Process Tech 214(9):1871–1878. https://doi.org/10.1016/j.jmatprotec.2014.04.001
22. Huang C, Zhou M, Zhang H (2021) A cutting force prediction model in axial ultrasonic vibration end grinding for BK7 optical glass considering protrusion height of abrasive grits. Measurement 180:109512. https://doi.org/10.1016/j.measurement.2021.109512
23. Feng G, Guo JB, Zhang GJ (2020) Material removal characteristics of ultra-precision grinding silicon carbide ceramics. Adv Appl Ceram 119(4):175–182. https://doi.org/10.1080/17436753.2019.1707414

24. Hu ZW, Chen Y, Lai ZY, Yu YQ, Xu XP, Peng Q, Zhang L (2022) Coupling of double grains enforces the grinding process in vibration-assisted scratch: insights from molecular dynamics. J Mater Process Tech 304:117551. https://doi.org/10.1016/j.jmatprotec.2022.117551
25. Yu TB, Zhang TQ, Yu XM, Yang XZ, Sun JY (2019) Study on optimization of ultrasonic-vibration-assisted polishing process parameters. Measurement 135:651–660. https://doi.org/10.1016/j.measurement.2018.12.008
26. Sharma V, Pandey PM (2016) Optimization of machining and vibration parameters for residual stresses minimization in ultrasonic assisted turning of 4340 hardened steel. Ultrasonics 70:172–182. https://doi.org/10.1016/j.ultras.2016.05.001
27. Wang Y, Lin B, Zhang X (2014) Research on the system matching model in ultrasonic vibration-assisted grinding. INT J ADV MANUF TECH 70(1–4):449–458. https://doi.org/10.1007/s00170-013-5269-2
28. Sun SY, Tang JY, Shao W, Cheng CS, Liu YX (2019) Research on the matching relationship between ultrasonic-assisted grinding parameters and workpiece surface roughness. Int J Adv Manuf Tech 102(1–4):487–496. https://doi.org/10.1007/s00170-018-3195-z
29. Lee W, Lin C (2017) Optimization of ultrasonic machining for fabricating square holes using the Taguchi methods. J Chin Inst Eng 40(5):421–427. https://doi.org/10.1080/02533839.2017.1326846
30. CAO Y, Zhu YJ, Ding WF, Qiu YT, Wang LF, Xu JH (2022) Vibration coupling effects and machining behavior of ultrasonic vibration plate device for creep-feed grinding of Inconel 718 nickel-based superalloy. Chin J Aeronaut 35(2):332–345. https://doi.org/10.1016/j.cja.2020.12.039
31. Li Z, Yuan SM, Ma J, Shen J, Batako AD (2021) Study on the surface formation mechanism in scratching test with different ultrasonic vibration forms. J Mater Process Tech 294:117108. https://doi.org/10.1016/j.jmatprotec.2021.117108
32. Cao JG, Wu YB, Lu D, Fujimoto M, Nomura M (2014) Material removal behavior in ultrasonic-assisted scratching of SiC ceramics with a single diamond tool. Int J Mach Tool Manu 79:49–61. https://doi.org/10.1016/j.ijmachtools.2014.02.002
33. Duan N, Yu YQ, Shi WB, Xiao Q, Liu Q (2021) Investigation on diamond damaged process during a single-scratch of single crystal silicon carbide. Wear 486–487. https://doi.org/10.1016/j.wear.2021.204099
34. Wang PZ, Ge PQ, Ge MR, Bi WB, Meng JF (2019) Material removal mechanism and crack propagation in single scratch and double scratch tests of single-crystal silicon carbide by abrasives on wire saw. Ceram Int 45(1):384–393. https://doi.org/10.1016/j.ceramint.2018.09.178
35. Dai JB, Su HH, Zhou WB, Zhang QL, Zheng YH (2019) Experimental and numerical investigation on the interference of diamond grains in double-grain grinding silicon carbide ceramics. J Manuf Process 44:408–417. https://doi.org/10.1016/j.jmapro.2019.06.014
36. Chen Y, Hu ZW, Jin JF, Li L, Yu YQ, Peng Q, Xu XP (2021) Molecular dynamics simulations of scratching characteristics in vibration-assisted nano-scratch of single-crystal silicon. Appl Surf Sci 551:149451. https://doi.org/10.1016/j.apsusc.2021.149451
37. Steve P (1995) Fast parallel algorithms for short-range molecular dynamics. J Comput Phys 117:1–19. https://doi.org/10.1006/jcph.1995.1039
38. Stukowski A (2010) Visualization and analysis of atomistic simulation data with OVITO–the Open visualization Tool. Model Simul Mater Sc 18(1):015012. https://doi.org/10.1088/0965-0393/18/1/015012
39. Tersoff J (1989) Modeling solid-state chemistry: interatomic potentials for multicomponent systems. Phys Rev B 39(8):5566–5568. https://doi.org/10.1103/physrevb.39.5566
40. Malkin S, Sons (1989) Grinding technology: theory and application of machining with abrasives, John Wiley & Sons, pp. 59. https://doi.org/10.1016/0890-6955(91)90088-K
41. Li HB, Chen T, Duan ZY, Zhang YW, Li HT (2022) A grinding force model in two-dimensional ultrasonic-assisted grinding of silicon carbide. J Mater Process Tech 04:117568. https://doi.org/10.1016/j.jmatprotec.2022.117568
42. Zheng K, Liao WH, Sun LJ, Heng M (2019) Investigation on grinding temperature in ultrasonic vibration-assisted grinding of zirconia ceramics. Mach Sci Technol 23(4):612–628. https://doi.org/10.1080/10910344.2019.1575405
43. Hauke J, Kossowski TM (2011) Comparison of values of Pearson's and Spearman's correlation coefficients on the same sets of data. Quaest Geogr 30(2):87–93. https://doi.org/10.2478/v10117-011-0021-1